

# Broadband Transverse Electric Surface Wave in Silicene

M. Shoufie Ukhtary,<sup>1, a)</sup> Ahmad R. T. Nugraha,<sup>1</sup> Eddwi H. Hasdeo,<sup>1</sup> and Riichiro Saito<sup>1</sup>

*Department of Physics, Tohoku University, Sendai 980-8578, Japan*

(Dated: 4 March 2024)

Transverse electric (TE) surface wave in silicene is theoretically investigated. The TE surface wave in silicene is found to exhibit better characteristics compared with that in graphene, in terms of a broader frequency range and more confinement to the surface which originate from the buckled structure of silicene. We found that even undoped silicene can support the TE surface wave. We expect to obtain the similar characteristics of the TE surface wave in other two-dimensional materials that have slightly buckled honeycomb lattice.

PACS numbers: 72.20.Pa, 72.10.-d, 73.50.Lw

Surface electromagnetic waves, or simply surface waves are electromagnetic (EM) waves that propagate on the surface of a material<sup>1</sup>. Surface waves recently have attracted a lot of interest, because of their capability to transport the EM energy on the surface<sup>1-6</sup>. There are two kinds of surface waves based on their polarizations; the transverse magnetic (TM) and transverse electric (TE) surface waves. In the case of TM surface wave, the component of magnetic field is transverse to the propagation direction, while the electric field has a component parallel to the propagation direction. The TM surface wave that also refers to a surface plasmon, can be seen as an electric dipole wave on the surface of material due to spatial perturbation of charge density<sup>7,8</sup>. On the other hand, the TE surface wave has the component of electric field transverse to the propagation direction while the magnetic field has a component parallel to the direction of propagation. The TE surface wave can be seen as a magnetic dipole wave on the surface of material due to the self-sustained surface current oscillation<sup>7,8</sup>.

It is important to note that the radiation loss of magnetic dipole is much smaller than that of electric dipole<sup>9</sup>. Therefore, the TE surface wave can propagate longer than TM surface wave<sup>10,11</sup>, which makes the TE surface wave desirable for the transporting EM energy over long distance<sup>7,11</sup>. However, the TE surface wave cannot exist on the surface of an conventional bulk metal because condition for generating the TE mode is limited which means that the induced surface current is not available in the conventional bulk metal<sup>1,2,7,12</sup>. Some efforts have been made for designing artificial materials so that the TE surface wave can be generated, such as metamaterials and a cluster of nanoparticles, which are generally complicated, hence making them less viable and accessible<sup>3,7,11,13</sup>.

The difficulties of generating the TE surface wave can be alleviated by using two-dimensional (2D) materials such like graphene, which is a monolayer of carbon atoms arranged in honeycomb lattice<sup>14,15</sup>. Mikhailov and Ziegler have shown that, when the imaginary part of optical conductivity of 2D material is negative (posi-

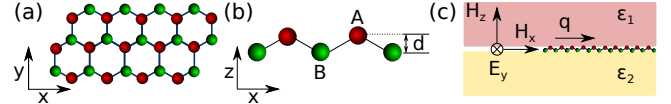


FIG. 1. (a) Honeycomb lattice of silicene. (b) Silicene lattice from side view. Sublattice A (B) is depicted by red (green) atom. (c) Silicene is sandwiched between two dielectric media. TE surface wave propagates on the surface of silicene with wave vector  $q$ . The electric field  $E_y$  is perpendicular to  $q$ .

itive), the TE (TM) surface wave can propagate on the surface of the 2D materials<sup>15</sup>. Due to the presence of the Dirac cone in its electronic structure, the imaginary part of optical conductivity of graphene can be negative at a certain frequency range. This is in contrast to usual 2D electron gas systems, which have a positive imaginary part of optical conductivity<sup>10,15</sup>. This unusual property has also enabled graphene to have the TE surface wave<sup>8,10,15,16</sup>. However, it was predicted that the TE surface wave in doped graphene may only exist for a narrow frequency range of  $1.667E_F < \hbar\omega < 2E_F$ <sup>8,10,15</sup>, where  $E_F$  is the Fermi energy. Moreover, the TE surface wave in graphene is less confined in the direction perpendicular to the surface in comparison with the TM surface wave<sup>10,15</sup>.

In this letter, we propose that silicene is a better 2D material rather than graphene to support the TE surface wave. Silicene is a monolayer of silicon atoms arranged in honeycomb lattice and the stable structure of silicene is not purely planar, but slightly buckled<sup>17-20</sup>, i.e., the two sublattices are separated by vertical distance  $d = 0.46 \text{ \AA}$  due to the  $sp^3$ -like hybridization<sup>20,21</sup>. The schematic structure of silicene can be seen in Figs. 1(a) and 1(b). The buckling of the atoms creates potential difference between two sublattices when an external electric field is applied in the direction perpendicular to the surface<sup>17-20</sup>. The induced potential difference, along with the non-negligible spin orbit (SO) coupling in silicene, will give a tunable energy gap<sup>17,18,20,22</sup>. We will show that the tunable energy gap of silicene affects a unique optical conductivity and the properties of TE surface wave which makes it a key difference from graphene.

Suppose that a silicene layer, or generally any mono-

<sup>a)</sup> Electronic mail: shoufie@flex.phys.tohoku.ac.jp

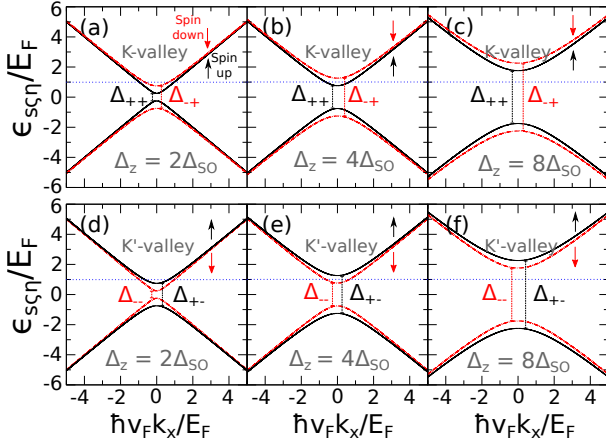


FIG. 2. Electronic energy dispersions of silicene for [(a)-(c)] K and [(d)-(f)] K' valleys for several  $\Delta_z$ 's ( $2\Delta_{SO}$ ,  $4\Delta_{SO}$ , and  $8\Delta_{SO}$ ). The solid (dash-dotted) lines correspond to spin up (down) electron dispersion. Positions of  $E_F = 7.8$  meV are indicated by the horizontal dotted lines.

layer 2D material, in the  $x-y$  plane is sandwiched between two dielectric media with dielectric constant  $\varepsilon_1$  and  $\varepsilon_2$  as shown in Fig. 1(c). The dispersion of the TE surface wave can be obtained by employing the Maxwell equations with boundary conditions of TE wave near the surface of the layer. Here we assume that the 2D material is negligibly thin and it is characterized by its optical conductivity  $\sigma$  which will appear as a surface current density in the boundary conditions for magnetic field as shown below. The TE surface wave has an electric field  $E_y$  in the  $y$  direction and the wave vector  $q$  in the  $x$  direction. There are two magnetic field components  $H_x$  and  $H_z$  in TE surface wave as shown in Fig. 1(c). Due to the confined nature of the surface wave, the EM fields should decay in the direction perpendicular to the surface ( $z$ ). Thus, we can write the magnetic fields in the media 1 and 2 as  $H_x^{(1)}(x, z) = A_1 \exp(-\kappa_1 z + iqx)$  and  $H_x^{(2)}(x, z) = A_2 \exp(\kappa_2 z + iqx)$ , respectively. The electric field in the  $k$ -th medium ( $k = 1, 2$ ) is obtained through  $E_y^{(k)}(x, z) = -i\omega\mu_0 \int H_x^{(k)}(x, z) dz$ . The decay constant  $\kappa_k$  is given by  $\kappa_k = \sqrt{q^2 - \varepsilon_k(\omega/c)^2}$ . The boundary conditions at the surface are (i)  $E_y^{(2)} - E_y^{(1)} = 0$  and (ii)  $(H_x^{(2)} - H_x^{(1)}) = J$ , where  $J = \sigma E_y$  is defined as surface current density. Employing the boundary conditions and assuming that the two dielectric media as vacuum ( $\varepsilon_1 = \varepsilon_2 = 1$ , thus  $\kappa_1 = \kappa_2 = \sqrt{q^2 - (\omega/c)^2} \equiv \kappa$ ), we obtain the TE surface wave dispersion<sup>15,16</sup>,

$$2 - \frac{i\sigma(\omega)\omega\mu_0}{\kappa} = 0. \quad (1)$$

Since  $\omega$  is a positive value, Eq. (1) requires a negative value of  $\text{Im } \sigma$ .

Next, we derive the  $\sigma(\omega)$  of silicene. Similar to graphene, the behavior of electrons at low-energy can be described by the Dirac Hamiltonian near the K and K'

points (hexagonal corners of Brillouin zone)<sup>17-20</sup>. However, we should consider the following two factors: (1) the SO coupling in silicene is much larger than that of graphene<sup>17,18,22</sup>, and (2) the potential difference between the sublattices A and B can be induced by an external perpendicular electric field  $E_z$ <sup>17-20</sup>. The Hamiltonian of silicene can be written in the following matrix form,

$$\hat{H}_{\varsigma\eta} = \begin{bmatrix} -\frac{1}{2}\varsigma\eta\Delta_{SO} + \frac{1}{2}\Delta_z & \hbar v_F(\eta k_x - i k_y) \\ \hbar v_F(\eta k_x + i k_y) & \frac{1}{2}\varsigma\eta\Delta_{SO} - \frac{1}{2}\Delta_z \end{bmatrix}, \quad (2)$$

where  $v_F$  is the Fermi velocity of electron and it is  $5.5 \times 10^5$  m/s for silicene<sup>22</sup>. The Hamiltonian is spin and valley dependent, labeled by  $\varsigma = +1(-1)$  for spin up (spin down) and  $\eta = +1(-1)$  for K (K') valley.  $\Delta_{SO} \approx 3.9$  meV represents the SO coupling for silicene<sup>20</sup> and  $\Delta_z = eE_z d$  denotes the potential difference between sublattices.  $d = 0.46$  Å denotes the vertical distance between the A and B atoms shown in Fig. 1(b). The eigenvalues of Eq. (2) are expressed by  $\epsilon_{\varsigma\eta}(k) = (-1)^{s+1}\epsilon_{\varsigma\eta}(k)$ , with  $s$  is 1 and 2 for the conduction and valence band, respectively.  $\epsilon_{\varsigma\eta}(k)$  is the energy dispersion for electron with  $\varsigma$  spin and at  $\eta$  valley, which is given by

$$\epsilon_{\varsigma\eta}(k) = \sqrt{(\hbar v_F k)^2 + \frac{1}{4}\Delta_{\varsigma\eta}^2}, \quad (3)$$

where  $k = \sqrt{k_x^2 + k_y^2}$  and  $\Delta_{\varsigma\eta}(\Delta_z) = |\Delta_z - \varsigma\eta\Delta_{SO}|$  denotes the energy gap which is tunable by applying the  $E_z$  up to  $2.6$  V Å<sup>-1</sup> where the structure of silicene becomes unstable<sup>23</sup>. The energy gap is defined as the energy separation from the top of the valence band to the bottom of the conduction band with the same spin sign. There are only two distinct values of  $\Delta_{\varsigma\eta}(\Delta_z)$  for four possible combination of  $\Delta_{\varsigma\eta}$ , since  $\Delta_{++}(\Delta_z) = \Delta_{--}(\Delta_z)$  and  $\Delta_{+-}(\Delta_z) = \Delta_{-+}(\Delta_z)$ .

The optical conductivity  $\sigma(\omega)$  of silicene can be obtained by the Kubo formalism for current-current correlation function<sup>24,25</sup>. The electron scattering is ignored here. Following the derivation of graphene's conductivity by Falkovsky and Varlamov,  $\sigma_{\varsigma\eta}$  can be expressed by<sup>24</sup>,

$$\sigma_{\varsigma\eta}(\omega) = -\frac{ie^2}{4\omega\pi^2} \left\{ \sum_s \int d^2k [v_{ss}^x(k)]^2 \frac{df[\epsilon_{s\varsigma\eta}]}{d\epsilon_{s\varsigma\eta}} \right\} + \frac{i\omega e^2}{2\pi^2} \hbar^2 \left\{ \int d^2k \frac{f[\epsilon_{1\varsigma\eta}(k)] - f[\epsilon_{2\varsigma\eta}(k)]}{\epsilon_{2\varsigma\eta}(k) - \epsilon_{1\varsigma\eta}(k)} \frac{v_{12}^x(k)v_{21}^x(k)}{\hbar^2\omega^2 - [\epsilon_{2\varsigma\eta}(k) - \epsilon_{1\varsigma\eta}(k)]^2} \right\}, \quad (4)$$

where  $f[\epsilon]$  is the Fermi distribution function and  $v_{ss'}$  is the matrix element of velocity matrix  $\hat{v}(k) = U^{-1}(\partial H_{\varsigma\eta}(\mathbf{k})/\hbar\partial\mathbf{k})U$  in the  $x$  direction, where  $U$  is the unitary matrix which diagonalize  $H_{\varsigma\eta}$ . The  $\hat{v}(k)$  matrix is explicitly given as follows:

$$\hat{v}(k) = \frac{\hbar v_F^2 k}{\epsilon_{\zeta\eta}} \begin{bmatrix} \hat{\mathbf{x}} \cos \theta + \hat{\mathbf{y}} \sin \theta & -Z_- \{ \hat{\mathbf{x}} \eta (-\Gamma_- + A_-) - \hat{\mathbf{y}} i (B_- - I_-) \} \\ Z_+ \{ \hat{\mathbf{x}} \eta (\Gamma_+ + A_+) - \hat{\mathbf{y}} i (B_+ + I_+) \} & -\hat{\mathbf{x}} \cos \theta - \hat{\mathbf{y}} \sin \theta \end{bmatrix}, \quad (5)$$

where we define  $\beta_{\pm} = \epsilon_{\zeta\eta} \pm 1/2\Delta_{\zeta\eta}$ ,  $Z_{\pm} = (\beta_{\pm}/\beta_{\mp})^{1/2}$ ,  $\Gamma_{\pm} = \Delta_{\zeta\eta} \cos \theta / \beta_{\pm}$ ,  $A_{\pm} = i2\epsilon_{\zeta\eta} \sin \theta / \beta_{\pm}$ ,  $B_{\pm} = 2\epsilon_{\zeta\eta} \cos \theta / \beta_{\pm}$ , and  $I_{\pm} = i2\Delta_{\zeta\eta} \sin \theta / \beta_{\pm}$ . Here  $\theta$  is the angle between  $k_x$  and  $k_y$ , while  $v_{nm}^x$  denotes the  $x$ -component of the  $n-m$  element of  $\hat{v}$  matrix. The first (second) term in Eq. (4) corresponds to the intraband (interband) conductivity, which is later labeled as  $\sigma_{\zeta\eta}^A$  ( $\sigma_{\zeta\eta}^E$ ).

By using Eqs. (3) and (5), we can calculate  $\sigma$  in Eq. (4) for silicene at  $T = 0$  K<sup>17,18</sup>. Here,  $\sigma$  is the total conductivity for both spin and valley degrees of freedom. For simplicity, we fix the  $E_F = 2\Delta_{SO} = 7.8$  meV, and vary the  $\Delta_z$ . Then, we get  $\sigma$  as follows

$$\sigma(\omega, \Delta_z) = \sum_{\zeta\eta} \{ \sigma_{\zeta\eta}^A(\omega, \Delta_z) + \sigma_{\zeta\eta}^E(\omega, \Delta_z) \}, \quad (6)$$

$$\sigma_{\zeta\eta}^A(\omega, \Delta_z) = i \frac{e^2}{16\hbar\pi} \frac{4E_F^2 - [\Delta_{\zeta\eta}(\Delta_z)]^2}{E_F \hbar\omega} \Theta[2E_F - \Delta_{\zeta\eta}(\Delta_z)] \quad (7)$$

$$\begin{aligned} \sigma_{\zeta\eta}^E(\omega, \Delta_z) = & \frac{e^2}{16\hbar} \left\{ 1 + \left( \frac{\Delta_{\zeta\eta}(\Delta_z)}{\hbar\omega} \right)^2 \right\} \Theta[\hbar\omega - g(\Delta_z)] \\ & - i \frac{e^2}{16\hbar\pi} \left\{ 1 + \left( \frac{\Delta_{\zeta\eta}(\Delta_z)}{\hbar\omega} \right)^2 \right\} \\ & \times \ln \left| \frac{\hbar\omega + g(\Delta_z)}{\hbar\omega - g(\Delta_z)} \right| + i \frac{e^2 [\Delta_{\zeta\eta}(\Delta_z)]^2}{8\hbar^2\pi\omega g(\Delta_z)}, \end{aligned} \quad (8)$$

where  $\Theta(x)$  is the Heaviside function and  $g(\Delta_z) = \max[2E_F, \Delta_{\zeta\eta}(\Delta_z)]$ . If we set  $\Delta_{\zeta\eta} = 0$ , we get the optical conductivity of graphene<sup>10,15</sup>.

In Fig. 2, we plot the electron energy dispersions for K and K' valleys based on Eq. (3) for several  $\Delta_z$ 's. In varying  $\Delta_z$ , we choose three cases for both the K and K' valleys depending on the position of  $E_F$  relative to the energy gap, which are shown in Fig. 2. The first case is  $\Delta_z = 2\Delta_{SO}$ , in which  $E_F$  is higher than bottoms of the two conduction bands for spin up and spin down ( $E_F > \Delta_{++/-}$  and  $\Delta_{-+/-}$ ) [Figs. 2(a) and 2(d)]. The second case is  $\Delta_z = 4\Delta_{SO}$ , in which  $E_F$  lies between two bottoms of the conduction bands ( $\Delta_{++/-} < E_F < \Delta_{-+/-}$ ) [Figs. 2(b) and 2(e)] and the third case is  $\Delta_z = 8\Delta_{SO}$ , in which  $E_F$  exists in energy gaps [Figs. 2(c) and 2(f)].

In Fig. 3, we plot the optical conductivity  $\sigma$  of silicene as a function of frequency where the solid and dashed lines are the imaginary and real parts of  $\sigma$ , respectively, for the three  $\Delta_z$ . We also plot the  $\sigma$  of graphene in black lines for a comparison. The logarithmic singularities in  $\text{Im } \sigma$  in Eq. (8) correspond to the lowest excitation energies for interband transitions

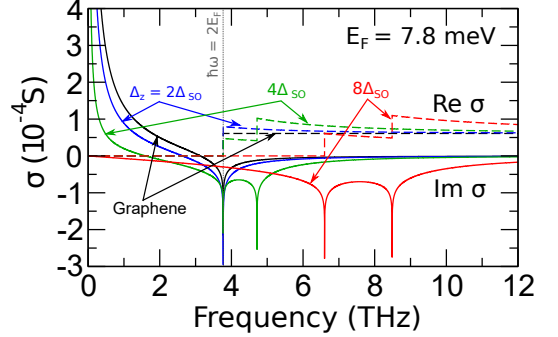


FIG. 3. Optical conductivity ( $\sigma$ ) of silicene for three different  $\Delta_z$  values and compared with that of graphene. The solid lines represent the imaginary part of  $\sigma$  and the dashed lines represent the real part of  $\sigma$ . Position of  $\hbar\omega = 2E_F$  is pointed at  $f = 3.77$  THz.

of electrons between energy bands having the same spin directions and the same valleys.  $\text{Im } \sigma$  is singular for any frequency which satisfies condition  $\hbar\omega = g(\Delta_z)$ . Since there are two distinct values of  $\Delta_{\zeta\eta}(\Delta_z)$ , there are two possible singularity points,  $\omega_1 = 2E_F/\hbar$  and  $\omega_2 = \Delta_{-+}/\hbar$  if  $\Delta_{++}/2 < E_F < \Delta_{-+}/2$  [ $\Delta_z = 4\Delta_{SO}$ ] or  $\omega_1 = \Delta_{++}/\hbar$  and  $\omega_2 = \Delta_{-+}/\hbar$  if  $E_F < \Delta_{++}/2$  and  $\Delta_{-+}/2$  [ $\Delta_z = 8\Delta_{SO}$ ]. When  $E_F > \Delta_{-+}/2$  and  $\Delta_{++}/2$  there is only one singularity point at  $\omega = 2E_F/\hbar$ . Since  $\sigma$  of silicene depends on  $\Delta_z$ ,  $\sigma$  of silicene can be tuned not only by  $E_F$  but also by  $E_z$ . As mentioned in Eq. (1), the negative value of  $\text{Im } \sigma$  correspond to the condition for TE surface wave. The TE surface wave cannot exist for the region that  $\text{Im } \sigma > 0$ . In the following discussion, we call the frequency range of  $\text{Im } \sigma < 0$  as the TE frequency range. Furthermore we focus only on the frequency range where  $\text{Re } \sigma = 0$  in which the TE surface wave is not damped<sup>15</sup>. For graphene ( $\Delta_{\zeta\eta} = 0$ ), the TE frequency range is fixed at  $1.667E_F < \hbar\omega < 2E_F$  ( $3.14 < f < 3.77$  THz), which reproduces the previous results<sup>10,15</sup>.

In general, the TE frequency range in silicene is wider than that in graphene for the same  $E_F$  and it is tunable by  $\Delta_z$  as shown in Fig. 3. For example, for  $\Delta_z = 2\Delta_{SO}$  ( $E_z = 16.96$  mVÅ<sup>-1</sup>), the TE frequency range lies within  $1.4E_F < \hbar\omega < 2E_F$  ( $2.64 < f < 3.77$  THz). By increasing  $\Delta_z$ ,  $\Delta_{\zeta\eta}$  increases. From Eq. (7)-(8) we know that increasing  $\Delta_{\zeta\eta}$  not only makes  $\text{Im } \sigma_{\zeta\eta}^E$  more negative, but also reduces  $\text{Im } \sigma_{\zeta\eta}^A$  whose value is always positive<sup>15</sup>. Altogether,  $\text{Im } \sigma$  decreases, hence the TE frequency range becomes wider when we increase  $\Delta_z$ . The  $\text{Im } \sigma_{\zeta\eta}^A$  can be suppressed when  $\Delta_{\zeta\eta} > 4\Delta_{SO}$ , or the Fermi level is located in  $\Delta_{\zeta\eta}$  [Figs. 2(b)-(c)].

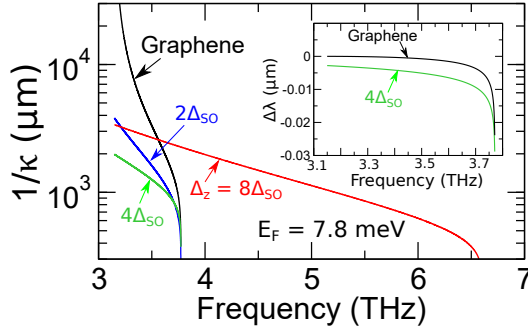


FIG. 4. Confinement length  $1/\kappa$  for silicene and graphene as a function of frequency. Inset :  $\Delta\lambda$  as a function of frequency for graphene and silicene.

This occurs for  $\Delta_z = 4\Delta_{\text{SO}}$  ( $E_z = 33.92 \text{ mV}\text{\AA}^{-1}$ ) and  $\Delta_z = 8\Delta_{\text{SO}}$  ( $E_z = 67.84 \text{ mV}\text{\AA}^{-1}$ ) (see Figs. 2(b) and (c) respectively). For  $\Delta_z = 4\Delta_{\text{SO}}$ , only  $\text{Im } \sigma_{+-}^A$  and  $\text{Im } \sigma_{-+}^A$  are suppressed, therefore we still have  $\text{Im } \sigma > 0$  at certain frequency and  $\text{Re } \sigma \neq 0$  for  $\hbar\omega \geq 2E_F$  ( $f \geq 3.77 \text{ THz}$ , see Eqs. (7) and (8)). Hence, the TE frequency range becomes  $1.61 < f < 3.77 \text{ THz}$ . But in the case of  $\Delta_z = 8\Delta_{\text{SO}}$ , all  $\text{Im } \sigma_{\pm\eta}^A$  vanish and  $\text{Im } \sigma$  has negative value at all frequency.  $\text{Re } \sigma \neq 0$  for  $\hbar\omega \geq \Delta_{++}$  ( $f \geq 6.60 \text{ THz}$ ). Therefore, the TE frequency range becomes  $0 < f < 6.60 \text{ THz}$ .  $\text{Re } \sigma$  appears at higher frequency than that for  $\Delta_z = 4\Delta_{\text{SO}}$ , because the Fermi level exists in all of the energy gaps, in which we need a higher excitation energy for interband transition.

Another interesting finding is that the undoped silicene ( $E_F = 0$ ) may also support TE surface wave. From Eqs. (6)–(8), for  $E_F = 0$  we get  $\text{Im } \sigma$ :

$$\text{Im } \sigma(\omega, \Delta_z) = -\frac{e^2}{16\hbar\pi} \sum_{\zeta\eta} \left\{ \left[ 1 + \left( \frac{\Delta_{\zeta\eta}(\Delta_z)}{\hbar\omega} \right)^2 \right] \times \ln \left| \frac{\hbar\omega + \Delta_{\zeta\eta}(\Delta_z)}{\hbar\omega - \Delta_{\zeta\eta}(\Delta_z)} \right| - \frac{2\Delta_{\zeta\eta}(\Delta_z)}{\hbar\omega} \right\}. \quad (9)$$

The TE frequency range lies within  $0 < \hbar\omega < \Delta_{++/-}$ . It is noted that  $\text{Im } \sigma(\omega)$  vanishes at  $E_F = 0$  in graphene<sup>15</sup>, hence the TE surface wave does not exist for undoped graphene.

From Eq. (1), we can define a confinement length of TE surface wave  $1/\kappa$ , as follows

$$\frac{1}{\kappa} = \frac{2}{i\omega\sigma(\omega, \Delta_z)\mu_0}. \quad (10)$$

A smaller value of  $1/\kappa$  corresponds to better confinement. In Fig. 4, we plot  $1/\kappa$  of the TE surface wave in graphene and silicene for comparison. The plot starts at  $f = 3.15 \text{ THz}$  ( $\hbar\omega = 1.667E_F$ ), which is the lower bound of TE frequency range in graphene. We can see that the TE surface wave in silicene is much more confined than in graphene and tunable by  $\Delta_z$ . For example, at  $f = 3.25 \text{ THz}$  ( $\hbar\omega = 1.725E_F$ ), in case of

graphene,  $1/\kappa = 13994 \text{ }\mu\text{m}$ , while in case of silicene,  $1/\kappa = 2906.2 \text{ }\mu\text{m}$  for  $\Delta_z = 2\Delta_{\text{SO}}$ ,  $1/\kappa = 1747.7 \text{ }\mu\text{m}$  for  $\Delta_z = 4\Delta_{\text{SO}}$ , and  $1/\kappa = 3146.7 \text{ }\mu\text{m}$  for  $\Delta_z = 8\Delta_{\text{SO}}$ . In the case of  $\Delta_z = 8\Delta_{\text{SO}}$ , we might get a larger  $1/\kappa$ . This is because  $\text{Im } \sigma$  is singular at higher frequency, which makes  $1/\kappa$  for  $\Delta_z = 8\Delta_{\text{SO}}$  slowly diverge.

By solving Eq. (1) for  $\lambda = 2\pi/q$ , we can define the difference between the wavelength of TE surface wave  $\lambda$  and the wavelength of freely propagating EM wave in vacuum  $\lambda_0 = 2\pi c/\omega$  as  $\Delta\lambda = \lambda - \lambda_0$ . In the inset of Fig. 4 we plot  $\Delta\lambda$  as a function of frequency for graphene and silicene with  $\Delta_z = 4\Delta_{\text{SO}}$ . We can see that  $\Delta\lambda$  is sufficiently small which means that  $\lambda$  is almost the same as  $\lambda_0$  (3 THz corresponds to  $\lambda_0 = 100\mu\text{m}$ ). However,  $\Delta\lambda$  for silicene is more negative compared with that for graphene, which is almost zero. Negative  $\Delta\lambda$  means that there is shrinkage of the wavelength of TE surface wave which is the preferable feature of surface wave since more information can be compressed in the wave. From the inset of Fig. 4, we can see more shrinkage of the wavelength in silicene compared with that in graphene.

In conclusion, silicene is theoretically proved to be a versatile platform for utilizing TE surface wave. We have shown that silicene supports the TE surface wave propagation and it exhibits more preferable surface wave properties compared with those of graphene, such as the tunable broadband frequency and smaller confinement length. The TE surface wave in silicene is tunable by the Fermi energy as well as by the external electric field. These characteristics originate from the two-dimensional buckled honeycomb structure.

M.S.U. and E.H.H. are supported by the MEXT scholarship. A.R.T.N. acknowledges the Leading Graduate School Program in Tohoku University. R.S. acknowledges MEXT (Japan) Grants No. 25107005 and No. 25286005.

- <sup>1</sup>W. T. Hill III and C. H. Lee, *Light-Matter Interaction* (Wiley-VCH, Weinheim, 2007).
- <sup>2</sup>S. A. Maier, M. L. Brongersma, P. G. Kik, S. Meltzer, A. A. G. Requicha, and H. A. Atwater, *Adv. Mater.* **13**, 1501 (2001).
- <sup>3</sup>H. Liu, D. A. Genov, D. M. Wu, Y. M. Liu, J. M. Steele, C. Sun, S. N. Zhu, and X. Zhang, *Phys. Rev. Lett.* **97**, 243902 (Dec 2006).
- <sup>4</sup>R. F. Oulton, V. J. Sorger, D. A. Genov, D. F. P. Pile, and X. Zhang, *Nature Photon.* **2**, 496 (2008).
- <sup>5</sup>A. Vakil and N. Engheta, *Science* **332**, 1291 (2011).
- <sup>6</sup>M. Jablan, H. Buljan, Y. Yin, and M. Soljačić, *Phys. Rev. B* **80**, 245435 (2009).
- <sup>7</sup>Z. Sun, X. Zuo, T. Guan, and W. Chen, *Opt. Express* **22**(4), 4714 (2014).
- <sup>8</sup>S. Menabde, D. Mason, E. Kornev, C. Lee, and N. Park, *Sci. Rep.* **6**, 21523 (2016).
- <sup>9</sup>J. D. Jackson, *Classical Electrodynamics* (Wiley-VCH, Weinheim, 1999).
- <sup>10</sup>X. Y. He and R. Li, *IEEE J. Sel. Top. Quantum Electron.* **20**, 62 (2014).
- <sup>11</sup>N. Liu, S. Mukherjee, K. Bao, Y. Li, L. V. Brown, P. Nordlander, and N. J. Halas, *ACS Nano* **6**, 5482 (2012).
- <sup>12</sup>D. Sarid and W. Challener, *Modern Introduction to Surface Plasmons: Theory, Mathematical Modeling, and Applications* (Cambridge University Press, Cambridge, 2010).
- <sup>13</sup>R. Ruppin, *Phys. Lett. A* **277**, 61 (2000).
- <sup>14</sup>K. S. Novoselov, A. K. Geim, S. V. Morozov, D. Jiang, M. I.

- Katsnelson, I. V. Grigorieva, S. V. Dubonos, and A. A. Firsov, Nature **438**, 197 (2005).
- <sup>15</sup>S. A. Mikhailov and K. Ziegler, Phys. Rev. Lett. **99**, 016803 (2007).
- <sup>16</sup>M. Jablan, H. Buljan, and M. Soljačić, Opt. Express **19**, 11236 (2011).
- <sup>17</sup>L. Stille, C. J. Tabert, and E. J. Nicol, Phys. Rev. B **86**, 195405 (2012).
- <sup>18</sup>C. J. Tabert and E. J. Nicol, Phys. Rev. B **89**, 195410 (2014).
- <sup>19</sup>G. G. Guzmán-Verri and L. C. L. Y. Voon, Phys. Rev. B **76**, 075131 (2007).
- <sup>20</sup>M. Ezawa, New J. P **14**, 033003 (2012).
- <sup>21</sup>C.-C. Liu, W. Feng, and Y. Yao, Phys. Rev. Lett. **107**, 076802 (2011).
- <sup>22</sup>C.-C. Liu, H. Jiang, and Y. Yao, Phys. Rev. B **84**, 195430 (2011).
- <sup>23</sup>N. D. Drummond, V. Zolyomi, and V. I. Fal'Ko, Phys. Rev. B **85**, 075423 (2012).
- <sup>24</sup>L. A. Falkovsky and A. A. Varlamov, EPJ B **56**, 281 (2007).
- <sup>25</sup>H. Bruus and K. Flensberg, *Many-body Quantum Theory in Condensed Matter Physics* (Oxford University Press, New York, 2004).